

INTERPLAY BETWEEN STELLAR SPIRALS AND THE ISM IN GALACTIC DISKS

KEIICHI WADA

Graduate School of Science and Engineering, Kagoshima University, Kagoshima, Japan

JUNICHI BABA

Center for Computational Astrophysics, National Astronomical Observatory of Japan

AND

TAKAYUKI R. SAITOH¹

National Astronomical Observatory of Japan

ABSTRACT

We propose a new dynamical picture of galactic stellar and gas spirals, based on hydrodynamic simulations in a ‘live’ stellar disk. We focus especially on spiral structures excited in a isolated galactic disk without a stellar bar. Using high-resolution, 3-dimensional N -body/SPH simulations, we found that the spiral features of the gas in galactic disks are formed by essentially different mechanisms from the galactic shock in stellar density waves. The stellar spiral arms and the interstellar matter on average corotate in a galactic potential at any radii. Unlike the stream motions in the galactic shock, the interstellar matter flows into the local potential minima with irregular motions. The flows converge to form dense gas clouds/filaments near the bottom of the stellar spirals, whose global structures resemble dust-lanes seen in late-type spiral galaxies. The stellar arms are non-steady; they are wound and stretched by the galactic shear, and thus local densities of the arm change on a time scale of ~ 100 Myrs, due to bifurcating or merging with other arms. This makes the gas spirals associated with the stellar arms non-steady. The association of dense gas clouds are eventually dissolved into inter-arm regions with non-circular motions. Star clusters are formed from the cold, dense gases, whose ages are less than ~ 30 Myrs, and they are roughly associated with the background stellar arms without a clear spatial offset between gas spiral arms and distribution of young stars.

Subject headings: galaxies: spiral — galaxies: ISM — ISM: kinematics and dynamics — methods: numerical

1. INTRODUCTION

Spiral structures are the most prominent features in disk galaxies, which can be excited by tidal interactions with companion galaxies (e.g. Oh et al. 2008; Dobbs et al. 2010; Struck et al. 2011) as well as by the central stellar bars (Sellwood & Sparke 1988; Binney & Tremaine 2008, (section 6.4)). Spiral structures can also be self-excited and maintained without the gravitational perturbations in globally stable disks as proposed by Lin & Shu (1964); They are interpreted as stationary density waves propagating in a stellar disk (see also Bertin & Lin 1996). In this paper, we focus on dynamics of the ISM in stellar spirals arisen in disk galaxies without external perturbations.

In the conventional picture, the stellar density waves generate spiral perturbations in a galactic potential. Dynamics of the interstellar medium (ISM) in the spiral potential have been theoretically studied since Fujimoto (1968), who found a standing shock, called a ‘galactic shock’, in a tightly wrapped spiral potential. Linear and non-linear behavior of the shock has been extensively studied from various perspectives (e.g., Roberts 1969; Shu et al. 1973; Woodward 1975; Norman 1978). The galactic spiral dust-lanes and associated star formation in the arms have since been regarded as a

consequence of the galactic shock. Although this is a widely accepted *static* picture of the galactic spiral, recent time-dependent, multi-dimensional simulations suggested that shocked layers in spiral potentials are not always dynamically stable (e.g., Kim et al. 2006; Shetty & Ostriker 2006; Dobbs & Bonnell 2006)². Spiral shocks can be hydrodynamically unstable (‘wobble instability’ (Wada & Koda 2004)), and sometimes form ‘spurs’ (Kim & Ostriker 2002). The substructures in the inter-arm regions are formed as a result of formation of clumps in the layers. In reality, various physics, such as self-gravity of the gas, radiative cooling, heating by stars, and the magnetic field could affect dynamics and structures of the ISM in a spiral potential (see Kim et al. 2010, and references therein). Using three-dimensional hydrodynamic simulations, taking into account the self-gravity of the gas and radiative cooling/heating processes and the supernova feedback, Wada (2008) found that the classic galactic shocks are unstable and transient, and that they migrate to globally quasi-steady, inhomogeneous arms due to nonlinear development of gravitational, thermal, and hydrodynamical instabilities.

One unrealistic assumption in most previous hydrodynamic and magneto-hydrodynamic simulations of galactic spirals is, however, that the spiral potential is ‘fixed’. Thus, dynamical interactions be-

wada@cfca.jp
baba.junichi@nao.ac.jp
saitoh.takayuki@nao.ac.jp

¹ JSPS fellow

² See also recent numerical simulations on tidally-driven spirals (Oh et al. 2008; Struck et al. 2011).

tween the gas and stellar components were not considered³. Yet, N -body simulations have shown that self-induced spiral structures in stellar disks are not stationary (Sellwood & Carlberg 1984; Sellwood 2000; Sellwood & Binney 2002; Fuchs et al. 2005; Fujii et al. 2011; Sellwood 2011). This is also the case in an N -body disk with a central bar (Baba et al. 2009). In any N -body models, amplitudes of spiral arms change on a time scale of galactic rotation, or even shorter. Stationary spiral waves with small pitch angles have never been numerically reproduced (Sellwood 2010, 2011). Each spiral arm in the N -body disk is transient, and recurrently reformed. Fujii et al. (2011) revealed a self-regulating mechanism that maintains multi-arm spiral features for at least 10 Gyrs in a pure stellar disk using three-dimensional N -body simulations. They showed that the dominant spiral modes are time-dependent, reflecting a highly non-linear evolution of spiral density enhancements.

What we should explore next is dynamical interactions between the ISM and the live (i.e. time-dependent) stellar disk. Interactions between the ISM and the stellar component in disk galaxies have been extensively studied since the 1970s, and it was suggested that the ISM is essential for dynamical structures in disk galaxies (e.g., Roberts & Shu 1972; Kalnajs 1972; Jog & Solomon 1984; Lin & Bertin 1985). However, fully non-linear evolution of the realistic multi-phase ISM in a live-stellar disk has not been investigated so far.

In this paper, we study dynamics of the multi-phase, self-gravitating gas in a self-induced stellar spiral arms in a galactic disk using Smoothed Particle Hydrodynamics (SPH) and N -body simulations. For comparison, a model using a fixed spiral potential is also presented. When radiative cooling and heating processes as well as the self-gravity of the gas are taken into account, it is essential to solve the whole three-dimensional disk; otherwise global non-axisymmetric, inhomogeneous structures and their evolution are not properly followed. We also implement ‘star’ formation from cold/dense gas and energy feedback from supernovae, by which we can study what triggers formation of young stars in the ISM in spiral arms.

One should note that the present simulations are not fully cosmological simulations, which are necessary to understand a full history of galaxy formation. Therefore, the numerical experiments here provide us with basic physical insight into dynamics of spiral arms in isolated late-type spiral galaxies at the present universe. Dynamics of spirals developed under an effect of the stellar bar will appear elsewhere (Baba et al. in prep.).

2. NUMERICAL METHODS AND MODEL SETUP

2.1. Methods

We used our original N -body/hydrodynamic simulation code **ASURA** (Saitoh et al. 2008, 2009) to solve the Newtonian equation of motions and the equations of hydrodynamics using the standard SPH methods (Lucy 1977; Gingold & Monaghan 1977; Springel 2010). The

numerical methods used here are the same as those in Baba et al. (2009, 2010). Here we briefly summarize them.

The self-gravity of stars and SPH particles is calculated by the Tree method with GRAPE (GRAVity PipE), a special purpose hardware for N -body simulations (Sugimoto et al. 1990). Here we used a software emulator of GRAPE, Phantom-GRAPE (Nitadori et al. in preparation). The gravitational softening length is 10 pc for both SPH and N -body particles.

We solve the energy equation implicitly with the cooling function (Spaans & Norman 1997; Wada & Norman 2001) assuming solar metallicity, in which various cooling processes⁴ are taken into account. Heating due to photoelectric heating of grains and polycyclic aromatic hydrocarbons (PAH) is considered, assuming a uniform far-ultraviolet radiation (FUV) with the $G_0 = 1.0$ in the Habing unit (Gerritsen & Icke 1997). We also implemented energy feedback from supernovae.

The treatment of star formation and the heating due to the SN feedback was the same as those in Saitoh et al. (2008, 2009). We adopted the simple stellar population (SSP) approximation, with the Salpeter initial mass function (Salpeter 1955) and the mass range of $0.1 - 100M_\odot$ is assumed. The local star formation rate (SFR), $d\rho_*/dt$, is assumed to be proportional to the local gas density, ρ_{gas} , and inversely proportional to the local dynamical time, $t_{\text{dyn}} \sim 1/\sqrt{G\rho_{\text{gas}}}$:

$$\frac{d\rho_*}{dt} = C_* \frac{\rho_{\text{gas}}}{t_{\text{dyn}}}, \quad (1)$$

where C_* is the dimensionless star formation efficiency parameter. The value of this parameter is usually calibrated by the global star formation properties, the Schmidt-Kennicutt relation (Kennicutt 1998; Martin & Kennicutt 2001). An SPH particle was replaced with a star particle following the Schmidt law (Schmidt 1959) with a local star formation efficiency $C_* = 0.033$ in a probabilistic manner (Saitoh et al. 2008, 2009; Robertson & Kravtsov 2008), if criteria (1) $n_{\text{H}} > 100 \text{ cm}^{-3}$, (2) $T < 100 \text{ K}$, and (3) $\nabla \cdot \vec{v} < 0$, are satisfied. Note that global (galactic) star formation rate is not directly proportional to the local star formation efficiency, C_* , but is rather controlled by the global evolution of the ISM (Saitoh et al. 2008).

We implemented type-II SN feedback, where the energy from SNe is injected to the gas around the star particles in the thermal energy. Each SN releases 10^{51} ergs of thermal energy for the surrounding SPH particles (typically 32 ± 2) particles. One gas particle ($m \sim 4000M_\odot$) produces about 30 SNe during 20 Myrs. This energy injection produces expanding cavities of hot gas ($T \sim 10^{6-7} \text{ K}$) in the ISM (see also section 2 in Saitoh & Makino 2010). Although the dynamics of the ISM on a galactic scale is mainly determined by the gravitational force, local structures of the ISM on a sub-kpc scale are affected by the feedback from SNe.

³ Dobbs & Bonnell (2006) used a time-dependent gravitational potential taken from an N -body simulations of Sellwood & Carlberg (1984), and ran 3-D, two-phase (i.e., cold and warm gas only) Smoothed Particle Hydrodynamics simulations.

⁴ (1) recombination of H, He, C, O, N, Si, and Fe; (2) collisional excitation of H_I, C_{I-IV}, and O_{I-IV}; (3) hydrogen and helium bremsstrahlung; (4) vibrational and rotational excitation of H₂; (5) atomic and molecular cooling due to fine-structure emission of C, C⁺, and O and rotational line emission of CO.

2.2. Live Spiral Model

We first evolve a pure N -body stellar disk with an exponential profile in a static dark matter (DM) halo potential whose density profile follows the Navarro-Frenk-White profile (Navarro et al. 1997). The initial stellar disk is generated using the Hernquist’s method (Hernquist 1993), and then it is evolved for a few Gyrs, randomizing azimuthal positions of stellar particles every several time-steps to prevent the growth of nonaxisymmetric features (McMillan & Dehnen 2007; Fujii et al. 2011). Figure 1 shows the initial circular velocity, velocity dispersions, and Toomre’s Q value as a function of the galactocentric distance. Once the stellar disk becomes almost featureless, we added a gaseous component, whose total mass is 10% of the stellar disk. This is regarded as an ‘initial’ condition in the result presented in §3. The model parameters of the DM halo, stellar disk, and gas disk are summarized in Table 1.

The total numbers of N -body and SPH particles are initially 3×10^6 and 10^6 , respectively. They are finally 3.2×10^6 and 0.8×10^6 , respectively. The corresponding particle masses are $11000 M_\odot$ and $3200 M_\odot$, respectively, owing to the star formation. Fujii et al. (2011) showed using pure N -body simulations that one million N -body particles are necessary to reproduce long-lived (> 10 Gyrs) spirals, and the results do not change in a model with $N = 3 \times 10^7$ particles. Saitoh et al. (2008) explored the effect of the numerical resolutions in ASURA in terms of representing inhomogeneous structures of the multi-phase gas on a galactic scale, and concluded that complicated structures of the multi-phase gas can be resolved with a particle mass of $3500 M_\odot$, or smaller. It was also confirmed that the results are converged between models with $3500 M_\odot$ and $350 M_\odot$.

2.3. Rigid Spiral Model

In order to study the effect of the live stellar disk, we run a test model, in which the stellar disk is replaced with a time-independent spiral potential. The gravitational potential of the stellar disk is

$$\begin{aligned} \Phi_{\text{sp}}(R, \phi, z) = & \Phi_{\text{disk},0}(R, z) \epsilon_{\text{sp}} \frac{z_0}{\sqrt{z^2 + z_0^2}} \\ & \times \cos \left[m \left(\phi + \cot i_{\text{sp}} \ln \frac{R}{R_0} \right) \right], \end{aligned} \quad (2)$$

on a rotating frame of the spirals. Here $\Phi_{\text{disk},0}$, m , ϵ_{sp} , i_{sp} , and z_0 are the axisymmetric potential produced by the stellar disk, the number of stellar spiral arms, the strength of the spiral perturbation, the pitch angle, and the scale-height, respectively. We set $i_{\text{sp}} = 30^\circ$, $m = 4$, and $\epsilon_{\text{sp}} = 0.02$. The phase is $R_0 = 1$ kpc and the pattern speed, Ω_{sp} , is $\simeq 12.2 \text{ km s}^{-1} \text{ kpc}^{-1}$ ($R_{\text{CR}} = 14$ kpc). These parameters are chosen from typical structures and dynamics of the live spiral model.

3. RESULTS

3.1. Non-steady Spiral Arms and Its Kinematics

Figure 2 shows four snapshots of V -band surface brightness reproduced by the stellar density during 975 Myrs. Obviously spiral arms are not stationary on a time scale of a few 100 Myrs (see also the movie in *the supplementary data*). If we track one of the spiral arms, we

Table 1

Model parameters for each mass component (dark matter halo, stellar disk, and gas disk). c_{NFW} is a concentration parameter in the Navarro-Frenk-White profile.

Component	Parameters	Value
Dark Matter Halo	Mass	$6.3 \times 10^{11} M_\odot$
	Radius	122 kpc
	c_{NFW}	5.0
Initial Stellar Disk	Mass	$3.2 \times 10^{10} M_\odot$
	Scale Length	4.3 kpc
	Scale Height	0.3 kpc
Initial Gas Disk	Mass	$3.2 \times 10^9 M_\odot$
	Scale Length	8.6 kpc
	Scale Height	0.1 kpc

observe that density of the arm is no longer constant – a part of the arm becomes faint or denser within one rotational period. There are no steady grand-design spiral arms, in fact spiral arms are ‘wound up’. Any arms are stretched by the galactic shear and attenuated. Splitting, bifurcating, and merging of arms are often observed. At the same time, new spiral arms are generated somewhere in the disk and as a result there are always several spiral arms in the disk. These phenomena suggest that the spiral arms do not propagate in the stellar disk as stationary density waves. In the present model, the number of spiral arms is 4-6, but the dominant modes are time- and radially-dependent (see also Fujii et al. 2011, for dynamical evolution of pure stellar spiral arms).

In the left panel of Figure 3, the rotational frequency of the most dominant mode of the spirals is shown as a function of radius at $t = 1.625$ Gyrs. It clearly shows that spiral arms mostly follow the galactic rotation $\Omega(R)$ at any radii. They do not rotate with a constant pattern speed. This is always the case during the evolution, as shown in the right three panels, in which time evolutions of stellar densities at three different radii, i.e. $R = 4.3, 8.6,$ and 12.9 kpc, are plotted. The inclination of black/gray stripes represents rotational speed of the spiral arms, showing that they basically follow the galactic rotation (red dashed line). Each stripe changes its shading in several 100 Myrs, indicating local density of the arm does change. The radially dependent rotational speed of spiral arms seems to be consistent with recent analysis of stellar kinematics in M51 and NGC 1068, in which a radially declining ‘pattern’ speed of spiral arms is found using the Tremaine-Weinberg method (Merrifield et al. 2006; Meidt et al. 2008). The numerical result clearly shows that spiral arms do not propagate as density waves with a single pattern speed in the disk, but they rather behave like ‘material’ arms⁵.

3.2. Behavior of the ISM in the Non-steady Spiral Potential

In these non-stationary stellar spiral arms, the structure and dynamics of the multi-phase ISM are quite dif-

⁵ Since the arms consist of stars, and the stars are not confined in each arm for many rotational periods, the spiral-like density enhancements also possess some similar properties in the ideal density waves. Detailed analysis of stellar orbits and their relationship to the non-steady spiral arms will be discussed elsewhere (Baba et al. in prep.).

ferent from the prevalent picture of the galactic shock. Figure 4 is a snapshot of cross-sections of the disk at three different galactic radii, revealing a typical azimuth distribution of stellar and densities. Relatively smooth curves represent azimuth distributions of the stellar density; for example there are four arms at $R = 8.6$ kpc and $6 \sim 7$ arms at $R = 12.9$ kpc at $t = 1.441$ Gyrs. Total gas density, on the other hand, is more spiky. Each peak corresponds to a high density clouds or internal substructures of them. It is clear that high density peaks of the gas tend to be associated with stellar arms. Moreover, this complicated structure of the gas is not steady (see also the movie in *the supplementary data*). These features are essentially different from the standing galactic shocks in a non-selfgravitating, isothermal gas in the spiral potentials.

The concentrations of cold ($T < 100$ K) gas seen in Fig. 4 actually form spiral structures in a two-dimensional distribution. Figure 5 shows distribution of the cold gas ($T < 100$ K) overlaid with the stellar density. It is clear that gas clouds roughly trace high density regions of stars, and they form complicated substructures in the stellar spirals. The associations of dense clumps can be traced as a single arm connected intermittently from the central region to the outer disk. As clearly seen in the movie in the supplementary data, a grand-design spiral arm of the gas is temporally formed, but it becomes sparse in a few ~ 100 Myrs.

As shown above, if the multi-arm stellar spirals are developed are developed by the swing amplification of density disturbances in the galactic disk (Toomre 1981; Fujii et al. 2011), both the gas and stellar arms follow the local galactic rotational velocity on average, and as a result the velocity of the gas relative to the stellar arms should be ~ 15 km s $^{-1}$ or smaller. On the rotating frame of the spiral arms, the ISM falls into the spiral potential from both sides, that is there are flows of cold gas slower and faster than the stellar arm. The flows converge into condensations of cold gas near the bottom of the potential well. The relative velocities of the gas to the stellar spirals are comparable to the random motion of the gas. In other words, the turbulent ISM ‘sub-sonically’ move near the spiral potential⁶. This is an essential difference in the flow in a time-independent spiral potential.

The converging gas flows near the spiral arms are clearly seen in a two-dimensional map, which is distinct from those in a rigid spiral potential. Figure 6 compares the velocity field of the cold gas ($T < 100$ K) between the live and rigid spiral potential models. In the live spiral model, the velocity vectors of the gas on a galactic rotation frame are irregular, and they tend to converge into the dense gas arms. In other words, since the relative velocity of the gas to the stellar spiral is small, the gas is ‘trapped’ by the potential troughs, forming high density regions. This is in contrast to what is observed in the rigid spiral model, where the potential is given as described in §2.2. The gas flows in the rigid spiral model are

relatively regular, and they change their directions near the gas arms, as typically seen in the two-dimensional galactic shock (Wada & Koda 2004). In both the models, supernova feedback is included, but this is not essential to change the velocity field of the gas near the spiral potential, although it sometimes dissolves the association of gas clouds (see §3.3). One should note here that the gas velocities relative to the spiral potential (here we assume that the live stellar arms follow the galactic rotation) are much slower than those in the rigid spiral model. In the right panel of Fig. 6, frequency distributions of the Mach number $\mathcal{M} \equiv |v|/c_s$ in both models are shown, where c_s is sound velocity, $c_s \equiv (\rho_g k T_g / \mu)^{1/2}$ with the gas density ρ_g and temperature T_g of each SPH particle, mean molecular mass μ , and $|v|$ is the gas local velocity on a galactic rotation (live spiral model) or on a rotating frame of the spiral potential (rigid spiral model). The sound velocity ranges from ~ 0.5 to ~ 300 km s $^{-1}$ depending on the local gas temperature. Therefore \mathcal{M} represents Mach number of the ISM relative to the spiral potential. It is clear that the gas flows in the rigid spiral potential are highly supersonic (i.e. $\mathcal{M} \sim 10 - 40$). On the other hand, in the live spiral model, the median is $\mathcal{M} \sim 2$. In Fig. 7, we plot the velocity field of the cold gas *relative to the galactic rotation*, i.e. mean background flow, in the rigid model. Although the median is $\mathcal{M} \sim 3$ and there are more gas with higher Mach number ($\mathcal{M} > 10$), the entire distributions of \mathcal{M} are similar in both model. Therefore it is reasonable that the local density field of the gas in both models are similar, showing filamentary and clumpy morphology.

If the converging gas flows of clumpy gas collide with low Mach number near the spiral arms, it could cause weak shocks *locally*. Weak shocks in warm gases near the stellar arms can trigger formation of molecular clouds through thermal instabilities (Inoue & Inutsuka 2009; Vazquez-Semadeni et al. 2011).

Each stellar arm becomes faint or merges into other arms on a time scale of the galactic rotation, or even shorter. Therefore one important aspect of the gas in the non-steady stellar spirals is that the gas concentrations, like giant molecular associations (GMA), formed in the potential troughs can obtain additional kinetic energy due to the variation of the background stellar spiral potential. This can be a source of dissolving the gas arms and generating kpc-scale non-circular motions of the ISM (Figure 6). We found that most of the cold gas clouds have large ‘epicyclic’ motions of which diameter is comparable to typical intervals between spirals arms, i.e. $\sim 2 - 3$ kpc. In other words, the gas circulates between spiral arms (see the movie in the supplementary data).

The large peculiar motions of the gas are in fact observed as proper motions of maser sources in our Galaxy (Reid et al. 2009). The observed peculiar motions of the star forming regions are quantitatively consistent with a numerical barred-spiral galaxy constructed by the same methods as those in the present paper (Baba et al. 2009). In Figure 8, an example of such a collision between cold streams is shown. The sequence of snapshots during 80 Myrs shows that concentrations of cold gas clumps, each of which is initially ~ 1 kpc away from the other, merge into one association of dense gas near the center of the stellar arm. The massive concentrations of cold

⁶ Effective sound speed, e.g. $\sqrt{c_s^2 + \sigma_v^2}$, where σ_v is velocity dispersion of the gas, can be larger than the thermal sound speed c_s especially for cold gas. Therefore the clumpy gas flow can be regarded as *sub-sonic* relative to the spiral arms, in other words, effective pressure of the turbulent gas could dominate dynamics of the flow near the spiral arms, even if the local Mach number is larger than unity (see discussion below).

gas, which would correspond to GMA in real galaxies, are temporarily formed and eventually dispersed as the background stellar arms become faint.

3.3. Star Formation and its Feedback in Spiral Arms

Here we implemented ‘star formation’ from cold, dense gas. Thus, collisions of dense gas clouds shown in Figure 6 may trigger star formation. Once the star particles are generated from their mother clouds based on the star-formation criteria described in §2, they behave as additional collisionless N -body particles (we call them ‘young stars’) in the live stellar disk. Figure 9 shows entire structures of old (i.e. disk stars) and young stars of which ages are less than 30 Myrs as well as the cold gas at $t = 1.6$ Gyrs. The young stars tend to form clusters along with the spiral arms consisting of old stars. However, there is no clear offset between young stars and the stellar spirals (i.e. gravitational potential), in contrast to the prediction of the galactic shock hypothesis. This is reasonable from the distribution and kinematics of cold, dense gas shown in Figs 4 and 5.

In Figures. 10 and 11, evolution of a spiral arm for a short period (20 Myrs) is shown by density and temperature maps, respectively. The gas clouds in the white circle around $R = 7.5$ kpc are cold ($T_g < 100$ K), and are surrounded by warm ($T_g \sim 10^3 - 10^5$ K), less dense gas. Around the cold clouds, several hot spots ($T_g \sim 10^6$ K) caused by supernovae appear, and the dense clouds are partially dissolved. Figure 12 shows a frequency distribution of ‘life time’ of high density gas, for randomly selected 1000 SPH particles. It shows that most gas particles do not keep $n_H > 100 \text{ cm}^{-3}$ for more than 10-20 Myrs. This reflects the fact that the high density clumps produce massive stars, and they are eventually destroyed by SNe originated in the clumps. Typically a 4000 M_\odot SPH particle produces about 30 SNe during 30 Myrs. As seen in Figure 9, gas filaments consisted of dense gas complexes in the stellar spiral arms produces clusters of massive stars, and energy feedback from SNe originated in the clusters sometimes trigger expanding motions of the gas clouds (see also the movies in the supplementary data).

3.4. Spurs

Many spiral galaxies, especially the ones with well defined primary dust-lanes, exhibit so called spurs and feathers (Elmegreen 1980; Scoville et al. 2001; La Vigne et al. 2006) On the other hand, although the gas spiral arms shows rich substructures, we do not see clear periodic spurs in the inter-arm regions in the present model (Fig.9). This is in contrast to results in previous hydrodynamic and magneto-hydrodynamic simulations where isothermal gas is evolved in a fixed spiral potential with a constant pattern speed, Ω_p (Kim & Ostriker 2002; Wada & Koda 2004; Shetty & Ostriker 2006; Dobbs & Bonnell 2006; Kim & Ostriker 2006). This implies that difference of rotational velocities between spiral potentials and the ISM is essential for forming the downstream spurs/feathers. In the present model, there are no strong shears or ordered motions of the gas in the live spiral model, because both the stellar spirals and the ISM follow the galactic rotation, i.e. $\Omega_p \sim \Omega(R)$. If $\Omega_p < \Omega(R)$, as suggested

by recent numerical simulations of tidally-excited spirals (Dobbs et al. 2010; Struck et al. 2011), spurs could be formed. This is consistent with that spurs tend to be clearly observed in well-defined two-arm spirals, such as M51 (Scoville et al. 2001).

4. CONCLUSIONS

We propose a new picture of galactic stellar and gas spirals, based on hydrodynamic simulations in a ‘live’ stellar disk. Here we focus on basic properties of multi-arm spiral structures in isolated disk galaxies without a central stellar bar. Tidally excited spirals in interacting galaxies are probably produced by the kinematic density wave (Kalnajs 1973) beyond scope of this paper (see e.g. Oh et al. 2008; Dobbs et al. 2010; Struck et al. 2011). In contrast to the theory of standing galactic shocks (e.g. Fujimoto 1968; Roberts 1969; Shu et al. 1972) in static spiral potentials caused by stellar density waves (Lin & Shu 1964; Bertin & Lin 1996), high-resolution, three-dimensional N -body/SPH simulations using the ASURA code (Saitoh et al. 2008) revealed non-steady and non-linear evolution of gas and stellar spirals. Morphology of the spiral structures looks similar to that seen in late-type spiral galaxies. Important features found in the numerical simulations and their implications are summarized as follows:

1. Rotational speeds of stellar spiral arms follow the galactic rotation. Grand-design spirals therefore cannot maintain their shapes over a rotational period. As a result they are wound up and torn off by the galactic shear. Spiral arms are recurrently formed, and often merge into other arms, by which local densities of the arm are no longer constant. This non-steady nature of spiral arms has been reported in 2-D and 3-D N -body simulations of pure stellar disks (e.g., Sellwood & Carlberg 1984; Sellwood 2011; Fujii et al. 2011). We confirmed that this is also the case in a stellar disk with the ISM.
2. The gas component on average also follows the galactic rotation. As a consequence, the Mach number of the gas relative to spiral potentials is around ~ 2 , while on the other hand, it is more than 10 in the rigid spiral model. Flows of cold, dense gas converge toward the stellar arms, resulting in formation of massive associations of the cold gas and star formation. This is an essential difference from the classical galactic shock, where the gas passes through the potential and forms a oblique, global shock along the spiral potential.
3. Most of the cold and dense gas clouds are associated with the time-dependent stellar spirals. The morphology of the gas spirals look similar to observed dust-lanes in multi-arm spiral galaxies. We, therefore, suspect that dust-lanes in late-type spiral galaxies, especially those in multi-arm spirals, are not galactic shocks.
4. Dense gas regions in the bottom of stellar arms are eventually dissolved into inter-arm regions. They are affected by variation of the background stellar spiral potential on a time scale of ~ 100 Myrs.

This can be a source of dissolving the gas arms and generating non-circular motion of the ISM. Energy feedback from supernovae also contributes to dissolve the complex of dense gas clumps. The entire motions of the cold gas on a galactic rotating frame are ‘epicyclic’, but whose radii are comparable to intervals between spiral arms.

5. The mechanism presented here may also explain complicated sub-structures of dust-lanes and distribution of molecular gas in spiral galaxies, such as M33 (Onodera et al. 2010; Gratier et al. 2010), or our Galaxy. In fact, Baba et al. (2010) showed using the same method that features in observed position-velocity diagrams of CO and HI in our Galaxy are identified as clumpy gas spiral arms.
6. In the model, stars are formed from cold, dense gases. Consequently, young stars, whose ages are less than 30 Myrs, form clusters, and they are associated with the background stellar arms. We do not see clear spatial offset between gas spiral arms and distribution of young stars.

The results above imply that it is essential to solve both live stellar disk and the multi-phase ISM self-consistently in order to understand dynamical structures in spiral galaxies and their evolution. If we change parameters of model galaxies, such as the rotation curve and disk mass, we can reproduce spiral galaxies with different morphology. It is also important to realize that structures in spiral galaxies should be ‘time-dependent’. Some differences in morphologies of isolated spiral galaxies, such as the number of spiral arms and substructures in spirals could be explained by evolutionary features. Barred spirals, in which $m = 2$ arms are driven by a stellar bar, will be separately discussed elsewhere (Baba et al., in prep).

The authors are grateful to J. Makino and E. Kokubo for stimulating discussions. We are also grateful to the referee for valuable comments. Numerical simulations were performed by Cray XT-4 in the Center for Computational Astrophysics (CfCA), National Astronomical Observatory of Japan. T.R.S. is financially supported by a Research Fellowship from the Japan Society for the Promotion of Science for Young Scientists.

REFERENCES

- Baba, J., Asaki, Y., Makino, J., Miyoshi, M., Saitoh, T. R., & Wada, K. 2009, *ApJ*, 706, 471
- Baba, J., Saitoh, T. R., & Wada, K. 2010, arXiv 1009.3096
- Bertin, G., & Lin, C. C. 1996, *Spiral structure in galaxies a density wave theory*, ed. G. Bertin & C. C. Lin
- Binney, J., & Tremaine, S. 2008, *Galactic Dynamics: Second Edition*, ed. Binney, J. & Tremaine, S. (Princeton University Press)
- Dobbs, C. L., & Bonnell, I. A. 2006, *MNRAS*, 367, 873
- Dobbs, C. L., Theis, C., Pringle, J. E., & Bate, M. R. 2010, *MNRAS*, 403, 625
- Elmegreen, D. M. 1980, *ApJ*, 242, 528
- Fioc, M., & Rocca-Volmerange, B. 1999, arXiv:astro-ph/9912179
- Fuchs, B., Dettbarn, C., & Tsuchiya, T. 2005, *A&A*, 444, 1
- Fujii, M. S., Baba, J., Saitoh, T. R., Makino, J., Kokubo, E., & Wada, K. 2011, *ApJ*, 730, 109
- Fujimoto, M. 1968, in *IAU Symposium*, Vol. 29, IAU Symposium, 453–+
- Gerritsen, J. P. E., & Icke, V. 1997, *A&A*, 325, 972
- Gingold, R. A., & Monaghan, J. J. 1977, *MNRAS*, 181, 375
- Gratier, P. et al. 2010, *A&A*, 522, A3+
- Hernquist, L. 1993, *ApJS*, 86, 389
- Inoue, T., & Inutsuka, S. 2009, *ApJ*, 704, 161
- Jog, C. J., & Solomon, P. M. 1984, *ApJ*, 276, 114
- Kalnajs, A. J. 1972, *Astrophys. Lett.*, 11, 41
- . 1973, *Proceedings of the Astronomical Society of Australia*, 2, 174
- Kennicutt, Jr., R. C. 1998, *ApJ*, 498, 541
- Kim, C., Kim, W., & Ostriker, E. C. 2006, *ApJ*, 649, L13
- . 2010, *ApJ*, 720, 1454
- Kim, W., & Ostriker, E. C. 2002, *ApJ*, 570, 132
- . 2006, *ApJ*, 646, 213
- La Vigne, M. A., Vogel, S. N., & Ostriker, E. C. 2006, *ApJ*, 650, 818
- Lin, C. C., & Bertin, G. 1985, in *IAU Symposium*, Vol. 106, *The Milky Way Galaxy*, ed. H. van Woerden, R. J. Allen, & W. B. Burton, 513–530
- Lin, C. C., & Shu, F. H. 1964, *ApJ*, 140, 646
- Lucy, L. B. 1977, *AJ*, 82, 1013
- Martin, C. L., & Kennicutt, Jr., R. C. 2001, *ApJ*, 555, 301
- McMillan, P. J., & Dehnen, W. 2007, *MNRAS*, 378, 541
- Navarro, J. F., Frenk, C. S., & White, S. D. M. 1997, *ApJ*, 490, 493
- Norman, C. A. 1978, *MNRAS*, 182, 457
- Oh, S. H., Kim, W., Lee, H. M., & Kim, J. 2008, *ApJ*, 683, 94
- Onodera, S. et al. 2010, *ApJ*, 722, L127
- Reid, M. J. et al. 2009, *ApJ*, 700, 137
- Roberts, W. W. 1969, *ApJ*, 158, 123
- Roberts, Jr., W. W., & Shu, F. H. 1972, *Astrophys. Lett.*, 12, 49
- Robertson, B. E., & Kravtsov, A. V. 2008, *ApJ*, 680, 1083
- Saitoh, T. R., Daisaka, H., Kokubo, E., Makino, J., Okamoto, T., Tomisaka, K., Wada, K., & Yoshida, N. 2008, *PASJ*, 60, 667
- . 2009, *PASJ*, 61, 481
- Saitoh, T. R., & Makino, J. 2010, *PASJ*, 62, 301
- Salpeter, E. E. 1955, *ApJ*, 121, 161
- Scoville, N. Z., Polletta, M., Ewald, S., Stolovy, S. R., Thompson, R., & Rieke, M. 2001, *AJ*, 122, 3017
- Sellwood, J. A. 2000, *Ap&SS*, 272, 31
- . 2010, ArXiv e-prints: 1006.4855
- . 2011, *MNRAS*, 410, 1637
- Sellwood, J. A., & Binney, J. J. 2002, *MNRAS*, 336, 785
- Sellwood, J. A., & Carlberg, R. G. 1984, *ApJ*, 282, 61
- Sellwood, J. A., & Sparke, L. S. 1988, *MNRAS*, 231, 25P
- Shetty, R., & Ostriker, E. C. 2006, *ApJ*, 647, 997
- Shu, F. H., Milione, V., Gebel, W., Yuan, C., Goldsmith, D. W., & Roberts, W. W. 1972, *ApJ*, 173, 557
- Shu, F. H., Milione, V., & Roberts, Jr., W. W. 1973, *ApJ*, 183, 819
- Spaans, M., & Norman, C. A. 1997, *ApJ*, 483, 87
- Springel, V. 2010, *ARA&A*, 48, 391
- Struck, C., Dobbs, C. L., & Hwang, J. 2011, ArXiv e-prints
- Sugimoto, D., Chikada, Y., Makino, J., Ito, T., Ebisuzaki, T., & Umemura, M. 1990, *Nature*, 345, 33
- Toomre, A. 1981, in *Structure and Evolution of Normal Galaxies*, ed. S. M. Fall & D. Lynden-Bell, 111–136
- Vazquez-Semadeni, E., Banerjee, R., Gomez, G., Hennebelle, P., Duffin, D., & Klessen, R. S. 2011, ArXiv e-prints: 1101.3384
- Wada, K. 2008, *ApJ*, 675, 188
- Wada, K., & Koda, J. 2004, *MNRAS*, 349, 270
- Wada, K., & Norman, C. A. 2001, *ApJ*, 547, 172
- Woodward, P. R. 1975, *ApJ*, 195, 61

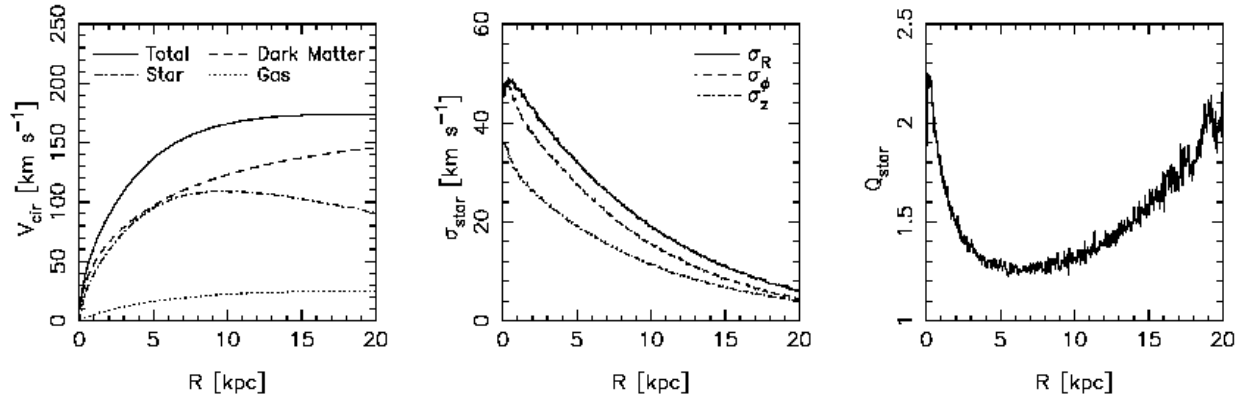


Figure 1. Initial condition of the stellar disk models in the live spiral model. (left) The circular velocity and contributions of individual component as a function of the galactocentric distance, R . (center) The velocity dispersions in the cylindrical coordinates (R, ϕ, z) as a function of R . (right) Toomre's Q value as a function of R .

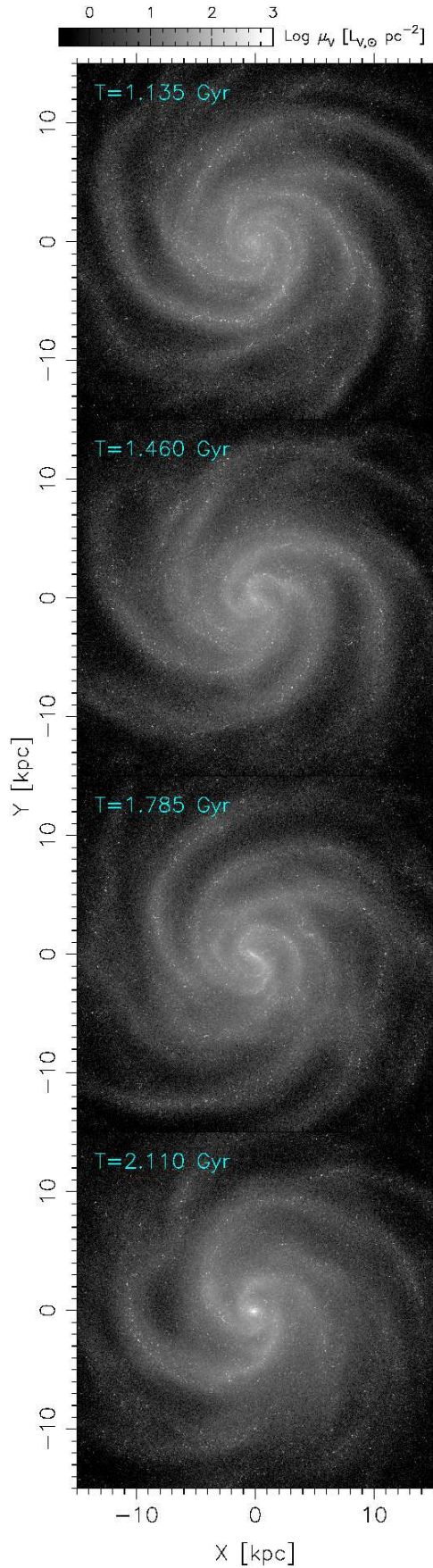


Figure 2. Evolution of stellar spirals on a rotation frame at $R = 8.6$ kpc. Gray-scale represents V-band surface luminosity calculated from stellar density with a population synthesis model, PEGASE.2 (Fioc & Rocca-Volmerange 1999), assuming a solar metallicity and the Salpeter initial mass function.

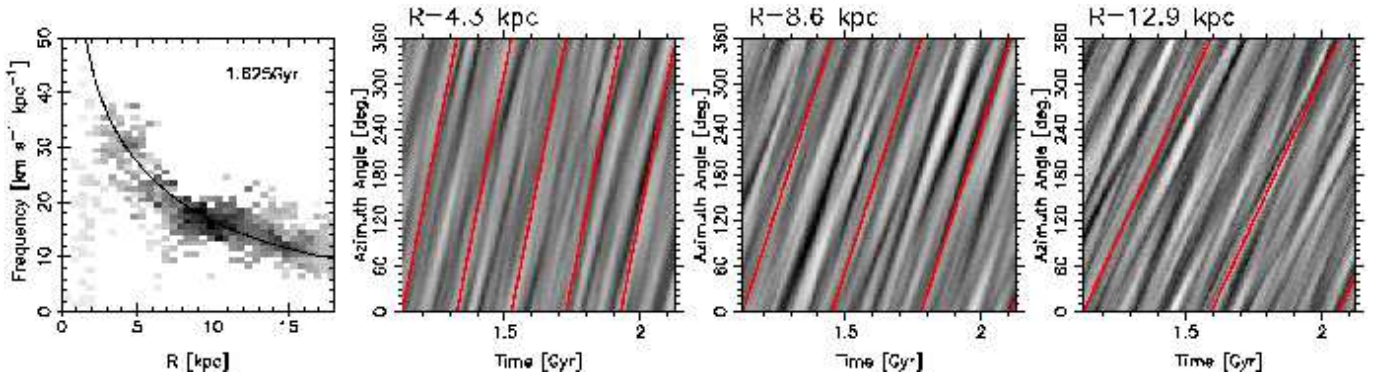


Figure 3. (left) Rotational frequency of the most dominant mode ($m = 4$) of the spirals is shown as a function radius at a snapshot of $t = 1.625$ Gyr. The gray scale represents the relative amplitude of the mode. The solid curve represents the circular frequency $\Omega(R)$. (right three panels) Kinematics of stellar arms at $R = 4.3, 8.6$ and 12.9 kpc. Black/gray stripes represent how the azimuthal positions of high density regions of stars move. The red solid lines represent the galactic rotation at each radius.

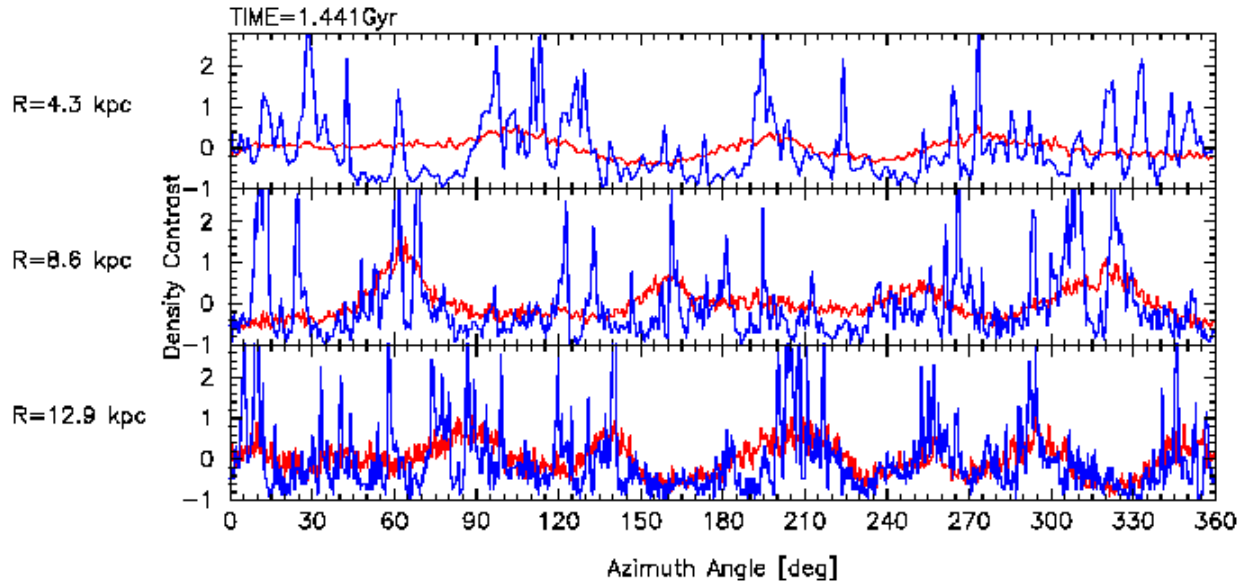


Figure 4. Azimuth distributions of stellar (red) and total gas (blue) density contrasts at $R = 4.3, 8.6$ and 12.9 kpc at $t = 1.441$ Gyr. See also the movie in the *supplementary data* for time evolution, where azimuthal density distributions are plotted on a rotating frame of a galactic rotation at each radius.

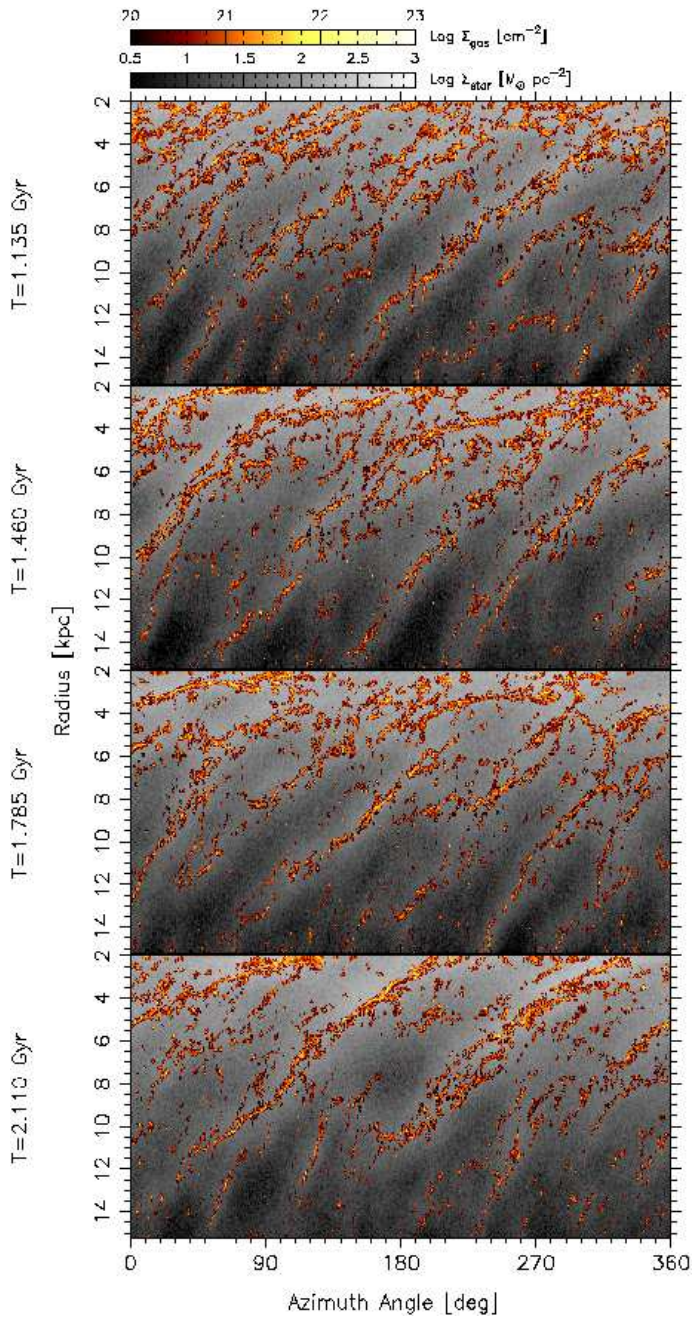


Figure 5. Cold gas ($T < 100$ K), whose surface density is represented by the color, is overlaid on a stellar density shown by a gray-scale. See also the movie in *the supplementary data*.

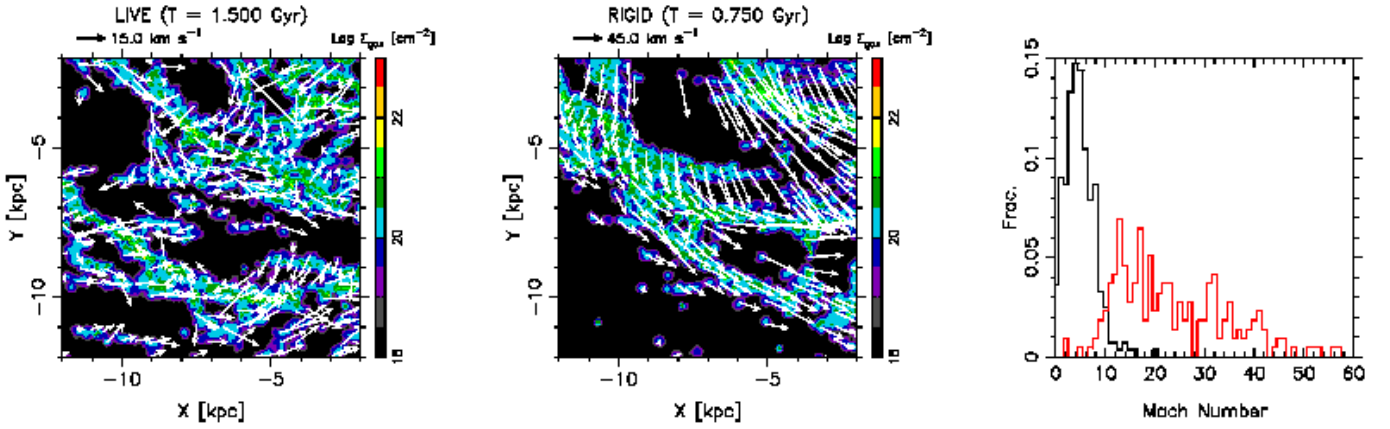


Figure 6. (left) Kinematics and surface density of the cold gas ($T < 100$ K) in the live spiral model. Arrows represent velocities of the gas relative to the galactic rotation, therefore they show approximately relative velocities to the local stellar spiral arms (see Fig. 3). Color represents gas density. (middle) Same as the left panel, but for the rigid spiral model. The velocities are on a rotating frame of the spiral potential. Note that unit length of the vectors in the two panels differ, and the velocities are much faster in the right two models than those in the live model. (right) Frequency distributions of the Mach number of SPH particles $\mathcal{M} \equiv |v|/c_s$ (see the text for the definition) in the live spiral model (black) and rigid spiral model (red).

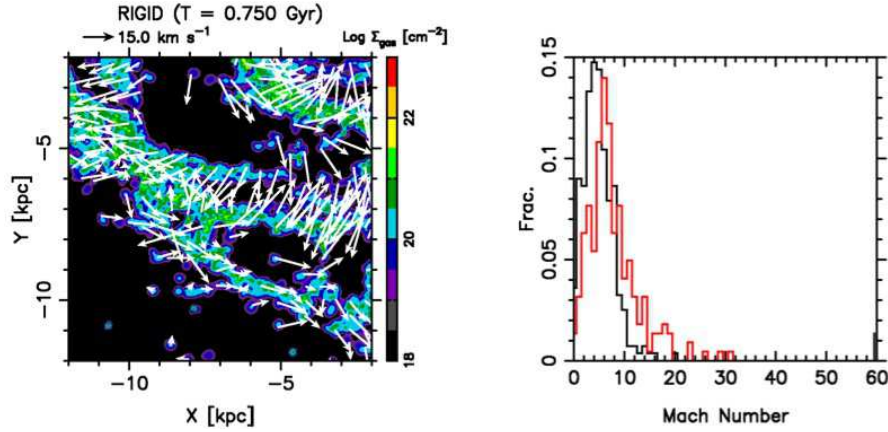


Figure 7. Same as the middle and right panels of Fig. 6, but the velocities are defined on the local galactic rotation.

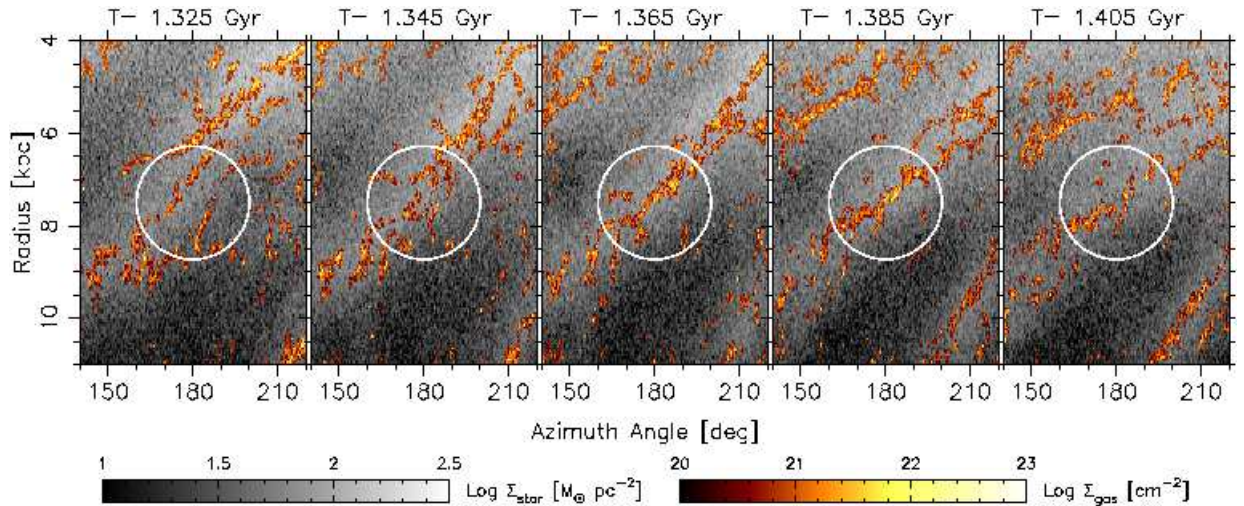


Figure 8. Same as Fig. 5, but a close-up of a collision of gas clouds near the stellar arm every 20 Myrs.

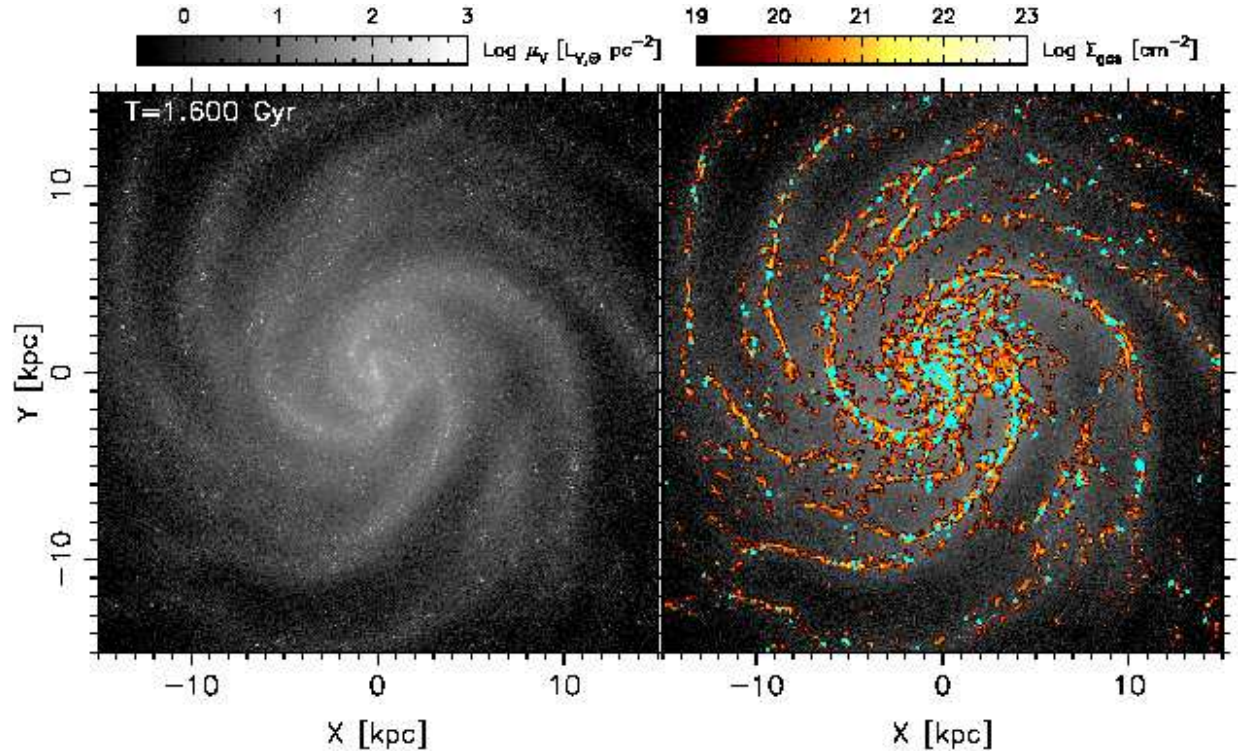


Figure 9. (Left) V -band surface luminosity calculated from stellar density with a population synthesis model. (Right) Cold gas ($T < 100$ K) density and star particles, whose ages are < 30 Myrs represented by light blue color, formed from cold, dense gas are overlaid on the left panel.

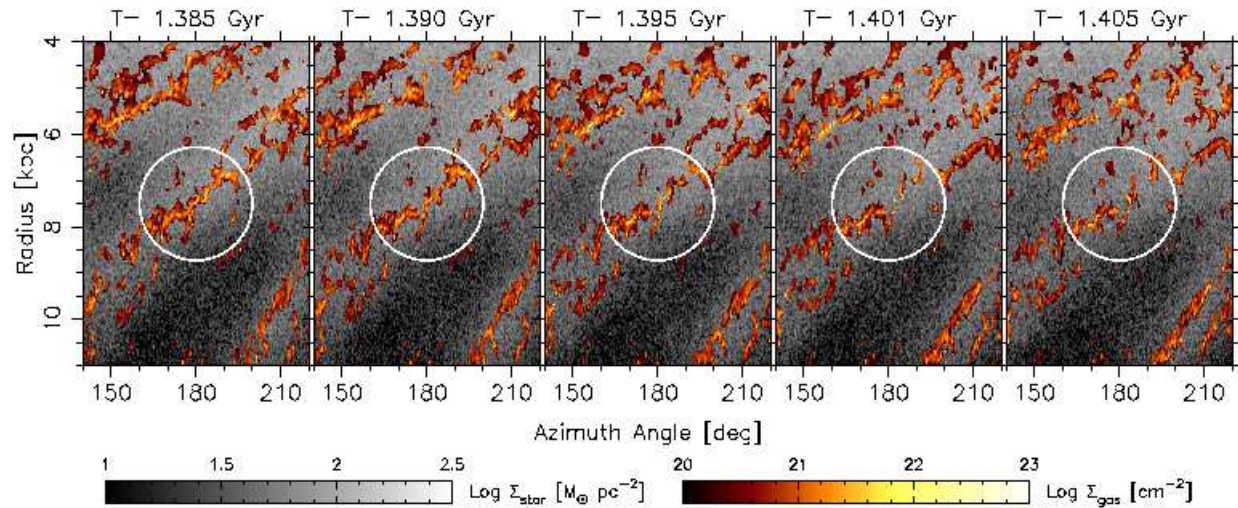


Figure 10. Same as Fig. 8, but snapshot every 5 Myrs after $t = 1.385$ Gyrs.

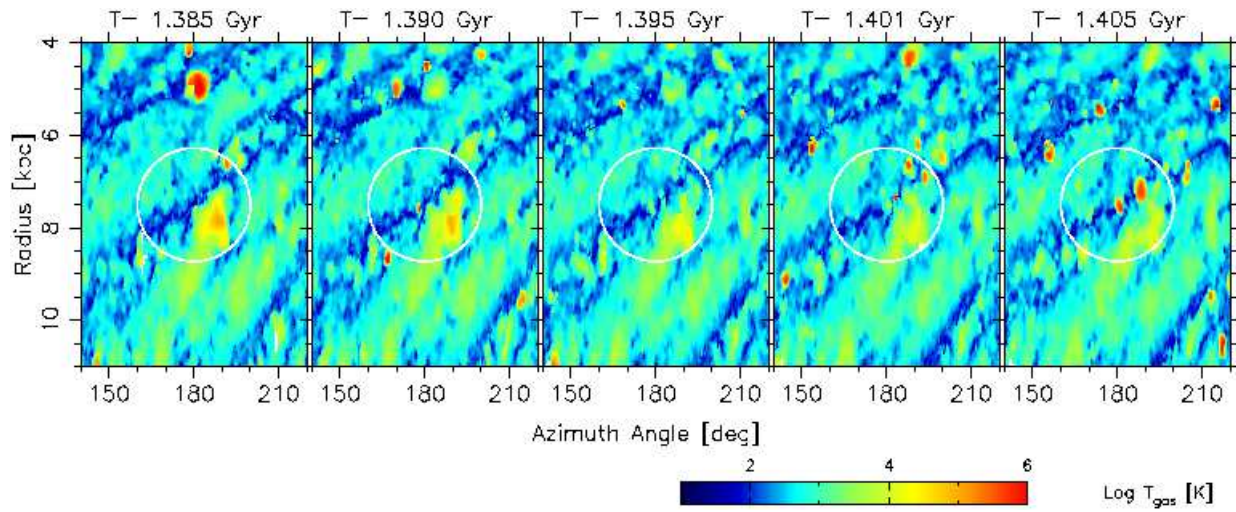


Figure 11. Same as Fig. 10, but temperature distribution. The hot regions (red) are generated by supernova explosions. (see also the movie in the supplementary data)

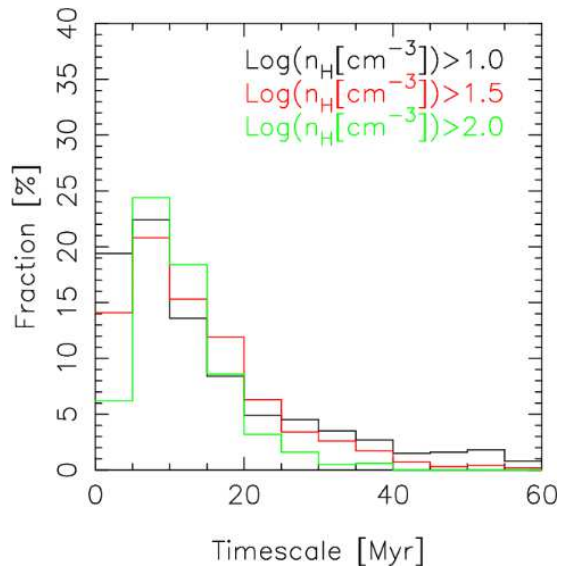


Figure 12. Frequency distribution of 'life time' to keep number densities, $n_{\text{H}} \geq 10, 10^{1.5}$ and 10^2 cm^{-3} .